

## Diffusion kurtosis as an in vivo imaging marker for reactive astrogliosis in traumatic brain injury

Jiachen Zhuo<sup>a,b,c</sup>, Su Xu<sup>a,b</sup>, Julie L. Proctor<sup>d</sup>, Roger J. Mullins<sup>b,e</sup>, Jonathan Z. Simon<sup>c,f</sup>, Gary Fiskum<sup>d</sup>, Rao P. Gullapalli<sup>a,b,\*</sup>

<sup>a</sup> Core for Translational Research in Imaging, University of Maryland School of Medicine, Baltimore, MD 21201, USA

<sup>b</sup> Department of Diagnostic Radiology & Nuclear Medicine, University of Maryland School of Medicine, Baltimore, MD 21201, USA

<sup>c</sup> Department of Electrical & Computer Engineering, University of Maryland, College Park, MD 20742, USA

<sup>d</sup> Department of Anesthesiology and Center for Shock Trauma and Anesthesiology Research, University of Maryland School of Medicine, Baltimore, MD 21201, USA

<sup>e</sup> Program in Neuroscience, University of Maryland School of Medicine, Baltimore, MD 21201, USA

<sup>f</sup> Department of Biology, University of Maryland, College Park, MD 20742, USA

### ARTICLE INFO

#### Article history:

Received 16 February 2011

Revised 11 July 2011

Accepted 14 July 2011

Available online 30 July 2011

#### Keywords:

Magnetic resonance imaging

Diffusion tensor imaging

Diffusion Kurtosis Imaging

Traumatic brain injury

Astrogliosis

Rat brain

### ABSTRACT

Diffusion Kurtosis Imaging (DKI) provides quantifiable information on the non-Gaussian behavior of water diffusion in biological tissue. Changes in water diffusion tensor imaging (DTI) parameters and DKI parameters in several white and gray matter regions were investigated in a mild controlled cortical impact (CCI) injury rat model at both the acute (2 h) and the sub-acute (7 days) stages following injury. Mixed model ANOVA analysis revealed significant changes in temporal patterns of both DTI and DKI parameters in the cortex, hippocampus, external capsule and corpus callosum. Post-hoc tests indicated acute changes in mean diffusivity (*MD*) in the bilateral cortex and hippocampus ( $p < 0.0005$ ) and fractional anisotropy (*FA*) in ipsilateral cortex ( $p < 0.0005$ ), hippocampus ( $p = 0.014$ ), corpus callosum ( $p = 0.031$ ) and contralateral external capsule ( $p = 0.011$ ). These changes returned to baseline by the sub-acute stage. However, mean kurtosis (*MK*) was significantly elevated at the sub-acute stages in all ipsilateral regions and scaled inversely with the distance from the impacted site (cortex and corpus callosum:  $p < 0.0005$ ; external capsule:  $p = 0.003$ ; hippocampus:  $p = 0.011$ ). Further, at the sub-acute stage increased *MK* was also observed in the contralateral regions compared to baseline (cortex:  $p = 0.032$ ; hippocampus:  $p = 0.039$ ) while no change was observed with *MD* and *FA*. An increase in mean kurtosis was associated with increased reactive astrogliosis from immunohistochemistry analysis. Our results suggest that DKI is sensitive to microstructural changes associated with reactive astrogliosis which may be missed by standard DTI parameters alone. Monitoring changes in *MK* allows the investigation of molecular and morphological changes in vivo due to reactive astrogliosis and may complement information available from standard DTI parameters. To date the use of diffusion tensor imaging has been limited to study changes in white matter integrity following traumatic insults. Given the sensitivity of DKI to detect microstructural changes even in the gray matter in vivo, allows the extension of the technique to understand patho-morphological changes in the whole brain following a traumatic insult.

© 2011 Elsevier Inc. All rights reserved.

### Introduction

Understanding tissue alterations at an early stage following traumatic brain injury (TBI) is critical for injury management and prevention of more severe secondary damage to the brain. Diffusion tensor imaging (DTI) is a powerful tool for studying neurological disease as it provides in vivo measurements of tissue microstructure change that could not otherwise be detected through conventional magnetic

resonance imaging (MRI) techniques. Diffusion of water protons in tissue is typically characterized by mean diffusivity (*MD*), which measures the average distance a water molecule traverses within a given observation time. Another parameter frequently derived from DTI data is fractional anisotropy (*FA*), which provides information on the degree of diffusion anisotropy existing within a given voxel. Studies using DTI have focused on white matter abnormality because of the highly directional diffusion of water found in the white matter tracts. In acute brain injuries, a reduced *MD* and/or increased *FA* has been equated with cellular swelling (cytotoxic edema) or increased cell density, leading to a reduced extra-cellular space (Armitage et al., 1998; Bazarian et al., 2007; Shanmuganathan et al., 2004) or brain tumor (Bulakbasi et al., 2003; Guo et al., 2002). At the same time, an increased *MD* and/or

\* Corresponding author at: Department of Diagnostic Radiology and Nuclear Medicine, University of Maryland School of Medicine, 22 South Greene Street, Baltimore, MD 21201, USA. Fax: +1 410 328 5937.

E-mail address: [rgullapalli@umm.edu](mailto:rgullapalli@umm.edu) (R.P. Gullapalli).

reduced  $FA$  has been equated with cellular membrane disruption, cell death, tissue cavitation, or vasogenic edema, which leads to an increased extra-cellular space as seen in patients with chronic brain injury (Cercignani et al., 2001; Wiesmann et al., 1999; Zelaya et al., 1999).

Although  $FA$  has been shown to be very sensitive in detecting subtle white matter microstructure changes following brain injury that correlate with clinical findings, two other parameters related to  $FA$ , namely the axial diffusivity ( $\lambda_a$ ) and radial diffusivity ( $\lambda_r$ ) provide further insights into the nature of the microstructural changes (Alexander et al., 2007; Chu et al., 2010; Newcombe et al., 2007). The axial component of the tensor,  $\lambda_a$  is believed to be sensitive to axonal injury, whereas the radial component,  $\lambda_r$  is thought to be sensitive to myelin integrity (Mac Donald et al., 2007; Sidaros et al., 2008; Song et al., 2003). Since the diffusion profile in the gray matter is considered to be largely isotropic (Pierpaoli et al., 1996), the use of DTI to study changes in the gray matter in brain injury has unfortunately received very little interest.

The diffusion of water in brain tissue, while complex, is largely simplified in a tensor model where the diffusion-weighted signal 'S' is assumed to follow a mono-exponential decay. The sensitization to the diffusion of water molecules in MRI is usually achieved by the use of bipolar gradients around the  $180^\circ$  pulse of a spin-echo, echo-planar imaging readout sequence. Typically for routine clinical evaluation, the b-values (a measure of the sensitivity to diffusion) in DTI experiments are around  $1000 \text{ s/mm}^2$  and can probe water diffusion changes over 50–100 ms. Observation of diffusion changes over this time frame provides sensitivity to a minimum diffusion distances of about 5–10  $\mu\text{m}$  (Assaf and Cohen, 2000). While this model is routinely used in the clinic, the model breaks down when higher b-values are used and the diffusion gradients are sensitized to probe restricted diffusion over shorter molecular distances (Assaf and Cohen, 1998; Niendorf et al., 1996). At such short molecular distances, the signal decay seen from diffusion-weighted imaging may deviate from mono-exponential decay as the technique becomes sensitive to even shorter molecular distances and increasingly sensitive to heterogeneous cellular structures especially in the radial direction as shown in Fig. 1 measured in the corpus callosum.

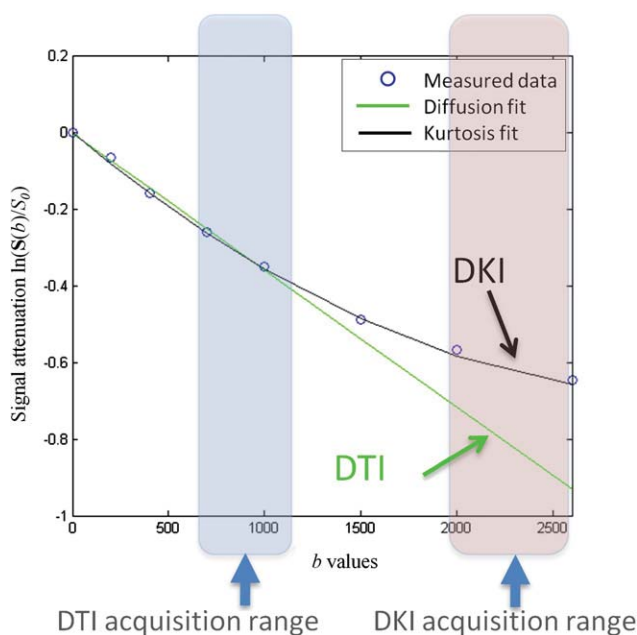


**Fig. 1.** The graph illustrates the errors associated with the assumption of Gaussian distribution of water diffusion as in the case of DTI reconstruction versus a non-Gaussian distribution assumption from DKI. Data were obtained from the corpus callosum using various b-values that were fit to both a linear equation as in the case of DTI and also fit to Eq. (1) for DKI. Note that when the b-values exceed  $1000 \text{ s/mm}^2$ , the data fits the DKI model significantly better than the DTI model.

This deviation from mono-exponential decay of the diffusion signal can potentially reveal more information about tissue microstructure changes, especially in structures such as the gray matter, tumor micro-environment (Raab et al., 2010), in regions of neurodegeneration (Farrell et al., 2010), and post traumatic tissue (Jiang et al., 2011), where heterogeneity may prevail. To understand such complex micro-environments, several models have been developed to characterize diffusion behavior. The most comprehensive and rigorous method proposed is the q-space method, which measures the diffusion weighted signal with different gradient strengths and diffusion times, and estimates the distribution of diffusion displacement of water (Cohen and Assaf, 2002). The q-space method thus provides a direct measure of water diffusion restriction in the tissue, which is indicative of cell size or axon radius (Cohen and Assaf, 2002; Farrell et al., 2010). However, the disadvantage of sampling using the complete q-space method is the extraordinarily long scan time and the extreme demand posed on imaging hardware, to reach a b-value as high as  $30,000 \text{ s/mm}^2$ , which is currently impractical on clinical scanners.

Other popular models include the bi-exponential model (Maier et al., 2004; Mulkern et al., 1999), and the diffusion kurtosis model (Jensen et al., 2005; Lu et al., 2006). The bi-exponential model describes the diffusion signal as resulting from both a fast and a slow compartment of water diffusion (Maier et al., 2001; Maier and Mulkern, 2008). However, compartmentalizing the tissue microenvironment may also be an oversimplification of the true nature of the tissue, since in reality the tissue may exhibit a continuum of diffusion distances rather than two discrete compartments (Kiselev and Il'yasov, 2007; Milne and Conradi, 2009).

The diffusion kurtosis model has been proposed as an alternative to the compartmental model, using a cumulant expansion of  $\ln(S)$  in a power series of  $b$  to fit the diffusion-weighted signal. This model makes no presumption of compartmentalization and has shown to fit the diffusion-weighted signal well, up to moderately large b-values of around  $2500 \text{ s/mm}^2$ . As seen in Fig. 1, the characteristics of the actual signal attenuation deviates from linear behavior after about  $b = 1000 \text{ s/mm}^2$  and is best captured by the kurtosis model especially when the b-value extends to a b value of  $2000 \text{ s/mm}^2$  or higher. Using this model, Diffusion Kurtosis Imaging (DKI) has shown great promise to better characterize gray matter microstructure change in rodent brain maturation (Cheung et al., 2009; Hui et al., 2008; Wu and Cheung, 2010) and in human brain aging (Falangola et al., 2008). Diffusion kurtosis has also shown to have clinical value in detecting tissue microstructure abnormality such as in squamous cell carcinoma (Jansen et al., 2010), cerebral gliomas (Raab et al., 2010), and lung dysfunction (Trampel et al., 2006). More specifically, diffusion kurtosis has been described as an imaging marker that captures brain tissue complexity (Jensen and Helpert, 2010; Shaw, 2010). Falangola et al. (2008) reported increased gray matter kurtosis with age, when moving from adolescence to adulthood, and attributed this increase to cortical cell-packing density, continuing myelination and an overall increase of the microstructural complexity in the brain. Earlier papers had determined the increased microstructural complexity with age to be related to increased activity of glial cells, which have a more complex cell structure than neurons (Terry et al., 1987). On the other hand, increased glial cell activity, or more specifically reactive astrogliosis, has long been used as reliable and sensitive pathology hallmark for diseased tissue in the central nervous system and for determining long-term clinical outcome from central nervous system injury (Chen et al., 2003; Sofroniew, 2009; Sofroniew and Vinters, 2010). Given the sensitivity of diffusion kurtosis to changes in tissue microstructure and possibly inflammation as a result of glial and astrocytic proliferation following brain injury we hypothesize that it may play an important role in detecting inflammatory changes following TBI. To test this hypothesis, we investigated the utility of diffusion kurtosis and compared its performance to standard diffusion tensor imaging parameters by monitoring changes in these parameters in a controlled compact injury (CCI) rat model at the acute

(2 h) stage and the sub-acute (7 days) stage and compared the findings with the tissue histopathology.

## Material and methods

### CCI TBI model

Adult male Sprague–Dawley rats ( $n = 12$ , 250–350 g) were subjected to left parietal CCI injury. Brain injury was induced using the controlled cortical impact device (Pittsburgh Precision Instruments, Pittsburgh, PA) as previously described (Dixon et al., 1991) with modified settings. Briefly, after being anesthetized initially with 4% isoflurane, the rats were maintained at 2% isoflurane throughout the procedure. The left parietal bone was exposed via a midline incision in a stereotactic frame. A high-speed dental drill (Henry Schein, Melville, NY) was used to perform a left-sided 5 mm craniotomy that was centered 3.5 mm posterior and 4 mm lateral to bregma. A 5 mm round impactor tip was accelerated to 5 m/s for an impact duration of 50 ms, resulting in a vertical deformation depth of 1.5 mm. The bone flap was immediately replaced with dental acrylic and the scalp incision was closed with silk. At the completion of surgery, isoflurane was discontinued, and rats were awakened and returned to their cages. Two additional sham rats (blank implanted) underwent identical surgeries, with the exclusion of the CCI. The experimental protocol was approved by the University of Maryland, Baltimore Institutional Animal Care and Use Committee.

### Imaging

All experiments were performed on a Bruker Biospec 7.0 Tesla 30 cm horizontal bore scanner (Bruker Biospin MRI GmbH, Germany) equipped with a BGA12S gradient system capable of producing pulse gradients of 400 mT/m in each of the three axes, with AVANCE III electronics and interfaced to a Bruker Paravision 5.0 console. A Bruker  $^1\text{H}$  4-channel surface coil array was used as the receiver and a Bruker 72 mm linear-volume coil as the transmitter. At all times during the experiment, the animal was under 1–2% isoflurane anesthesia and 1 L/min oxygen administration. Ear pins were used to reduce head motion and improve consistency in positioning the head for each animal. An MR compatible small-animal monitoring and gating system (SA Instruments, Inc., New York, USA) was used to monitor the animal respiration rate and body temperature. The animal body temperature was maintained at 36–37 °C using a warm water bath circulation. The total duration of the whole experiment was approximately 2 h. Each rat was imaged 1 day before injury and 2 h post-injury. Seven of the twelve rats were also imaged at 7 days post-injury while the other five rats were sacrificed at 48 h for histology for a separate study.

A three-slice (axial, mid-sagittal, and coronal) scout using rapid acquisition with fast low angle shot (FLASH) was used to localize the rat brain. A fast shimming procedure (Fastmap) was used to improve the  $B_0$  homogeneity within a region of the object. Both proton density (PD) and  $T_2$ -weighted images were obtained using a 2D rapid acquisition with relaxation enhancement (RARE) sequence in both the axial and coronal plane. Imaging was performed over a 3 cm field of view (FOV) in the coronal plane with an in-plane resolution of 117  $\mu\text{m}$  using 24 slices at 1 mm thickness with no gap, at an effective echo-time of 18.9 ms for the proton density weighted image and an effective echo-time of 56.8 ms for the  $T_2$ -weighted image. The echo-train length for each of the echoes was 4 and the repeat time (TR) was 5500 ms with two averages for a total acquisition time of ~12 min. Imaging was also performed in the axial plane using the same imaging parameter as above but over a FOV of  $3.0 \times 3.2 \text{ cm}^2$ .

For the DKI acquisition, diffusion weighted images were acquired with single shot, spin-echo echo-planar imaging (EPI) sequence. An encoding scheme of 30 gradient directions was used with the duration

of each of the diffusion gradients ( $\delta$ ) being 4 ms with a temporal spacing of 23 ms ( $\Delta$ ) between the two diffusion gradients. Two  $b$ -values (1000  $\text{s}/\text{mm}^2$  and 2000  $\text{s}/\text{mm}^2$ ) were acquired for each direction following the acquisition of five images acquired at  $b = 0 \text{ s}/\text{mm}^2$ . The DKI images were obtained using two averages using the same FOV and slice positions as the axial PD/ $T_2$  images but at an in-plane resolution of 234  $\mu\text{m}$  at a TR/TE of 6000/50 ms respectively for a total acquisition time of about 13 min.

### Histology

At 7 days post-surgery, and after all imaging was complete, the seven rats were anesthetized with ketamine and transcatheterially perfused with 4% formaldehyde and 2.5% acrolein. The brains were extracted from the skull and placed in 30% sucrose. A freezing sliding microtome was used to obtain 35  $\mu\text{m}$  brain sections. Sections were held at  $-20 \text{ }^\circ\text{C}$  prior to the immunohistochemistry procedure.

Each of the 35  $\mu\text{m}$  sections was labeled with antibodies against glial fibrillary acidic protein (GFAP). Sections were rinsed multiple times with a 0.05 M KPBS buffer and then subjected to a 20 min wash in a 1% solution of sodium borohydride and incubated in the primary antibody (anti-GFAP, 1:150 K; Dako North America, Inc., Carpinteria, CA) diluted in 0.05 M KPBS + 0.4% Triton-X for 48 h. They were then incubated for the secondary antibody (1:600), also diluted in 0.05 M KPBS + 0.4% Triton-X, for 1 h. Sections were incubated in A/B solution (1:222) for 1 h, and then in a Ni-DAB solution with a 0.175 M sodium acetate buffer for 12 min. Resulting slices were then mounted on slides, dehydrated, and cover-slipped with DPX mounting media. The sections were examined with a Leica (Nussloch, Germany) DMRX microscope equipped with a Phase One (Copenhagen, Denmark) Power Phase digital camera. Histology was also obtained from the two rats subject to sham injury.

### Diffusion reconstruction

Diffusion weighted (DW) images from individual averages were corrected first for motion artifacts using the 3dvolreg command in AFNI (Analysis of Functional NeuroImages, <http://afni.nimh.nih.gov/afni>; Cox, 1996). The 2 averages of motion corrected DW images were then averaged and spatially smoothed using a Gaussian filter with a FWHM of 0.3 mm to increase the signal–noise ratio (SNR). DW signals from all three  $b$ -values ( $b = 0, 1000, 2000 \text{ s}/\text{mm}^2$ ) and 30 directions were then fitted voxel-wise using non-linear least squares fit to the equation:

$$\ln S(\mathbf{g}, b) = \ln S_0 - b \sum_{i=1}^3 \sum_{j=1}^3 g_i g_j D_{ij} + \frac{1}{6} b^2 \sum_{i=1}^3 \sum_{j=1}^3 \sum_{k=1}^3 \sum_{l=1}^3 g_i g_j g_k g_l K_{ijkl} \quad (1)$$

where,

- $\mathbf{g} = (g_1, g_2, g_3)$  is the unit-vector direction of the diffusion gradient.
- $S(\mathbf{g}, b)$  is the diffusion-weighted signal at a particular  $b$  value with direction  $\mathbf{g}$ .
- $S_0$  is the MR signal with no diffusion weighting ( $b = 0 \text{ s}/\text{mm}^2$ ) and is the average of all the five  $b = 0$  volumes that were acquired.
- $D_{ij}$  is element of the  $3 \times 3$  diffusion tensor (DT)  $\mathbf{D}$ .
- $K_{ijkl}$  is element of a  $3 \times 3 \times 3 \times 3$  4th order tensor.  $K_{ijkl}$  is related to elements  $W_{ijkl}$  of the diffusion kurtosis Tensor (KT)  $\mathbf{W}$  and the mean diffusivity  $MD$  ( $\text{mm}^2/\text{s}$ ) by:

$$K_{ijkl} = MD^2 \cdot W_{ijkl}. \quad (2)$$

Since  $\mathbf{D}$  and  $\mathbf{W}$  are both totally symmetric matrices, with 6 independent elements of the DT and 15 independent elements for KT,

a total of 21 parameters were fitted using Eq. (1). The apparent diffusion coefficient  $D_{app}(\mathbf{g})$  and apparent kurtosis  $K_{app}(\mathbf{g})$  for each direction  $\mathbf{g}$  were then calculated from:

$$D_{app}(\mathbf{g}) = \sum_{i=1}^3 \sum_{j=1}^3 g_i g_j D_{ij} \quad (3)$$

$$K_{app}(\mathbf{g}) = \frac{1}{D_{app}(\mathbf{g})^2} \sum_{i=1}^3 \sum_{j=1}^3 \sum_{k=1}^3 \sum_{l=1}^3 g_i g_j g_k g_l K_{ijkl}. \quad (4)$$

It should be noted that this is a slightly different approach than what has been proposed in previous published literature where  $D_{app}(\mathbf{g})$  and  $K_{app}(\mathbf{g})$  are fit for each direction and then fit for the DT,  $\mathbf{D}$  and KT,  $\mathbf{W}$  (Cheung et al., 2009; Hui et al., 2008; Jensen et al., 2005; Lu et al., 2006; Wu and Cheung, 2010). Our initial testing of these two approaches (Zhuo et al., 2011) indicated that fitting the tensors first resulted in less fitting errors and resulted in parametric maps that were less noisy.

The three eigenvalues  $\lambda_1, \lambda_2, \lambda_3$  ( $\lambda_1 \geq \lambda_2 \geq \lambda_3$ ) and the corresponding eigenvectors ( $e_1, e_2, e_3$ ) were derived through eigen-decomposition of the DT. Several diffusion parameters, such as mean diffusivity ( $MD$ ), fractional anisotropy ( $FA$ ), axial diffusivity ( $\lambda_a$ ) and radial diffusivity ( $\lambda_r$ ) were calculated as follows:

$$MD = \frac{\lambda_1 + \lambda_2 + \lambda_3}{3} \quad (5)$$

$$FA = \frac{\sqrt{3[(\lambda_1 - MD)^2 + (\lambda_2 - MD)^2 + (\lambda_3 - MD)^2]}}{\sqrt{2(\lambda_1^2 + \lambda_2^2 + \lambda_3^2)}} \quad (6)$$

$$\lambda_a = \lambda_1, \quad \lambda_r = \frac{\lambda_2 + \lambda_3}{2}. \quad (7)$$

Diffusion kurtosis related parameters were derived from the KT. The mean kurtosis  $MK$  was calculated by averaging the  $K_{app}$  in all  $N=30$  directions.

$$MK = \frac{1}{N} \sum_{i=1}^N (K_{app})_i \quad (8)$$

Axial kurtosis ( $K_a$ ) and radial kurtosis ( $K_r$ ), which characterize the kurtosis along the axial and radial diffusion directions, were derived as in Jensen and Helpern (2010) after first transforming  $\mathbf{W}$  to the coordinates defined by the three eigenvectors of the diffusion tensor as:

$$\hat{W}_{ijkl} = \sum_{i'=1}^3 \sum_{j'=1}^3 \sum_{k'=1}^3 \sum_{l'=1}^3 e_{i'} e_{j'} e_{k'} e_{l'} W_{i'j'k'l'} \quad (9)$$

$$K_a = \frac{(\lambda_1 + \lambda_2 + \lambda_3)^2}{9\lambda_1^2} \hat{W}_{1111} \quad (10)$$

$$K_r = G_1(\lambda_1, \lambda_2, \lambda_3) \hat{W}_{2222} + G_1(\lambda_1, \lambda_3, \lambda_2) \hat{W}_{3333} + G_2(\lambda_1, \lambda_2, \lambda_3) \hat{W}_{2233} \quad (11)$$

where

$$G_1(\lambda_1, \lambda_2, \lambda_3) = \frac{(\lambda_1 + \lambda_2 + \lambda_3)^2}{18\lambda_2(\lambda_2 - \lambda_3)^2} \left( 2\lambda_2 + \frac{\lambda_3^2 - 3\lambda_2\lambda_3}{\sqrt{\lambda_2\lambda_3}} \right) \quad (12)$$

and

$$G_2(\lambda_1, \lambda_2, \lambda_3) = \frac{(\lambda_1 + \lambda_2 + \lambda_3)^2}{3(\lambda_2 - \lambda_3)^2} \left( \frac{\lambda_2 + \lambda_3}{\sqrt{\lambda_2\lambda_3}} - 2 \right). \quad (13)$$

## ROI analysis

To assess the effectiveness of the DTI and DKI parameters, several brain regions were selected. Manually drawn regions of interest (ROI) were placed ipsilateral and contralateral to the injury in the cortex (CTX), hippocampus (HC), external capsule (EC) and the corpus callosum (CC) on 2–3 consecutive slices at around Bregma 2.12 mm–4.52 mm (Paxinos and Watson, 1986) as shown in Fig. 2. These regions were defined on the  $FA$  images while using the  $T_2$ -weighted image for anatomic reference. Mean and standard deviation values from each of the ROIs from the DT and KT maps were then computed. For all regions, mean  $MD$ ,  $FA$ ,  $MK$  values were measured. For white matter regions (bilateral EC and CC), the parameters  $\lambda_a$ ,  $\lambda_r$ ,  $K_a$ , and  $K_r$  were also measured. Note that voxels with  $MK < 0$  or  $MD > 1.5 \times 10^{-3}$  were excluded and did not contribute to the ROI. Negative  $MK$ s were dominantly observed in the cortex ipsilateral to the injury and were typically associated with extremely low diffusivities (or noise) or hemorrhage, leading to erroneous fit for  $K_{app}$  with a negative value. Rather than replacing the negative  $K_{app}$  values with 0, which does not accurately reflect the local water mobility environment, these pixels were ignored and did not contribute to the average value of any given ROI. Negative  $MK$ s were dominantly observed in the ipsilateral cortex region closer to the foci of the injury at the acute stage, leading to an exclusion of  $2.2 \pm 2.8\%$  of voxels (ranging from 0% to 11%) within the region. Similarly, because of our interest in the diffusion behavior of the surviving tissue, we used a  $MD$  threshold of  $1.5 \times 10^{-3}$  mm/s<sup>2</sup> to exclude very highly edematous regions given that the normal  $MD$  of the cortex is around  $(0.82 \pm 0.04) \times 10^{-3}$  mm/s<sup>2</sup>. Visual observation of each rat showed that most of these voxels were only in the ipsilateral cortex at the sub-acute stage which resulted in the elimination of  $22.8 \pm 20.7\%$  of voxels (range of 0–60%) within the ROI.

## Statistics analysis

For each of the measured parameters ( $FA$ ,  $MD$ ,  $MK$ ,  $\lambda_a$ ,  $\lambda_r$ ,  $K_a$ , and  $K_r$  depending on gray or white matter) and each ROI (CC and bilateral HC, CTX, EC), a mixed model ANOVA was performed with two degrees of freedom for time (fixed effect) and eleven degrees of freedom for subjects (rats) to test changes in the signal patterns with time for each of the measures using SAS 9.2. The significant P values from ANOVA were then corrected for multiple comparison across all parameters and ROIs using false discovery rate (FDR) (Benjamini and Hochberg, 1995) with a  $q(\text{FDR}) = 0.05$ . Following ANOVA, post-hoc tests with Tukey–Kramer correction were carried out to test for differences between the baseline and the different time points post-injury. All reported p values were corrected and statistical significance was deemed at  $p < 0.05$ .

## Results

All the animals survived the seven day trial following the CCI injury. Parametric maps of DT ( $MD$ ,  $FA$ ,  $\lambda_a$ , and  $\lambda_r$ ) and KT ( $MK$ ,  $K_a$ ,  $K_r$ ) were generated for each of the animals. Fig. 3 shows  $FA$ ,  $MD$  and  $MK$  maps from a representative rat before and after injury (see Eqs. (5), (6), and (8) respectively). All animals demonstrated a decreased  $MD$  and an increased  $FA$  at the site of injury at the initial time point which reversed by the sub-acute stage as seen by changes in  $MD$  and  $FA$  on their respective maps. Increased edema was also clearly observed in the  $MD$  maps, including the  $T_2$ -weighted images (not shown) on all animals by the sub-acute stage at the site of the injury. Increased  $MK$  was observed in and around the site of the injury in all animals at 2 h post injury, followed by normalization by 7 days but persisted diffusely surrounding the injury.

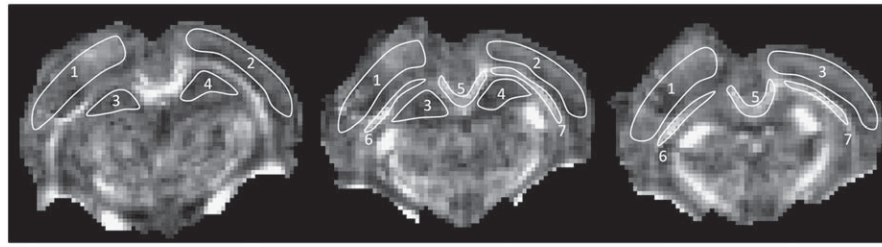


**Fig. 2.** Illustration of ROIs on FA maps for a representative injured rat on three consecutive coronal slices. Regions shown are: ipsi- (1) and contra- (2) lateral cortex, ipsi- (3) and contra- (4) lateral hippocampus, corpus callosum (5), ipsi- (6) and contra- (7) lateral external capsule.

*DTI changes following CCI*

Mixed model ANOVA revealed a significant temporal change in MD for bilateral hippocampus and cortex (HC\_ips:  $F_{2,11} = 50.31, p < 0.0001$ ; HC\_con:  $F_{2,11} = 16.69, p = 0.0007$ ; CTX\_ips:  $F_{2,11} = 70.98, p < 0.0001$ ; CTX\_con:  $F_{2,11} = 25.78, p < 0.0001$ ), where  $F_{2,11}$  is the F-score using two degrees of freedom for the imaging time points and eleven degrees of freedom for subjects (rats). These regions experienced a significantly reduced MD ( $p < 0.0005$ ) during the acute stage following CCI (Fig. 4) that tended to return to baseline by the sub-acute stage. Only the CTX\_ips demonstrated a significant increase in MD ( $p = 0.031$ ) compared to the baseline suggesting significant edema in this region.

For FA, the time effect was significant for HC\_ips ( $F_{2,11} = 12.06, p = 0.0028$ ), CTX\_ips ( $F_{2,11} = 26.96, p < 0.0001$ ), EC\_con ( $F_{2,11} = 5.85, p = 0.03$ ) and CC ( $F_{2,11} = 6.68, p = 0.02$ ). A significant increase in FA was observed in HC\_ips ( $p = 0.014$ ) and CTX\_ips ( $p < 0.0001$ ), while a significant decrease in FA was observed in EC\_con ( $p = 0.011$ ) and CC ( $p = 0.031$ ) at acute stage. These changes also returned to baseline levels by the sub-acute stage with the only exception being CTX\_ips where a significant reduction of FA was observed compared to the acute stage ( $p = 0.016$ ). The temporal change in FA within the EC\_ips was near significant ( $p = 0.08$ ) from ANOVA analysis but exhibited some variability probably due to the varying extent of injury between the rats at this site. Significant temporal changes for  $\lambda_a$  were observed in the EC\_con ( $F_{2,11} = 15.63, p = 0.001$ ) where  $\lambda_a$  was significantly

reduced ( $p = 0.0006$ ) at the acute stage which tended to return to the baseline by the sub-acute stage (Fig. 5). Changes in  $\lambda_r$  were not significant in any region.

*DKI changes following CCI*

The ipsilateral regions of the hippocampus ( $F_{2,11} = 6.27, p = 0.025$ ), cortex ( $F_{2,11} = 31.72, p < 0.0001$ ) and external capsule ( $F_{2,11} = 8.66, p = 0.009$ ) demonstrated a significant increase in MK over the 7 days of observation. Only the contralateral hippocampus ( $F_{2,11} = 11.47, p = 0.003$ ) and the cortex ( $F_{2,11} = 8.86, p = 0.008$ ) experienced significant increase in MK over 7 days. Temporal MK changes in the CC were also significant ( $F_{2,11} = 14.58, p = 0.02$ ). Significant increase in MK was observed in the CTX\_ips ( $p = 0.0002$ ) at the acute stage, and trend towards an increase was also observed in the HC\_ips ( $p = 0.09$ ). The signal abnormality in different regions at the sub-acute stage appeared to scale inversely with the distance from the impacted site, where CTX\_ips and CC showed the strongest increase in MK ( $p = 0.0002$ ), followed by EC\_ips ( $p = 0.003$ ), HC\_ips ( $p = 0.011$ ), CTX\_con ( $p = 0.032$ ) and HC\_con ( $p = 0.039$ ).

Significant changes with time were observed for  $K_a$  in the regions of EC\_ips ( $F_{2,11} = 12.11, p = 0.0028$ ) and CC ( $F_{2,11} = 6.66, p = 0.02$ ).  $K_a$  was significantly increased in EC\_ips ( $p = 0.013$ ) at the acute stage and stayed elevated at sub-acute stage ( $p = 0.0032$ ) as shown in Fig. 5.

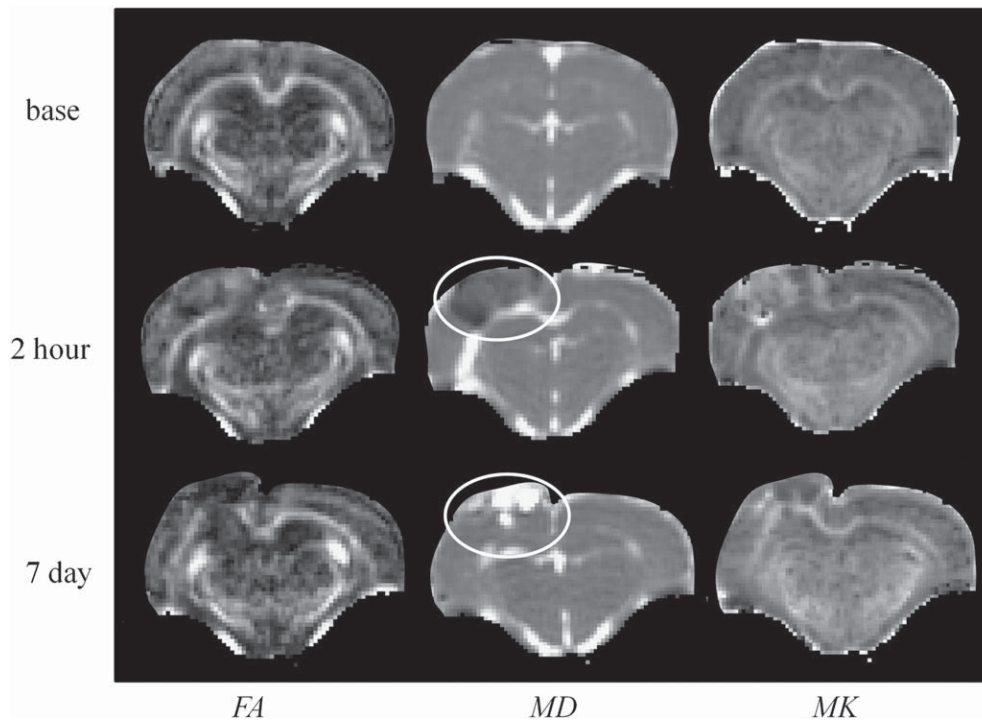


**Fig. 3.** FA, MD, and MK maps of a representative rat in the coronal view at baseline (pre-injury), 2 h and 7 days post injury. Circles indicate the site of injury.

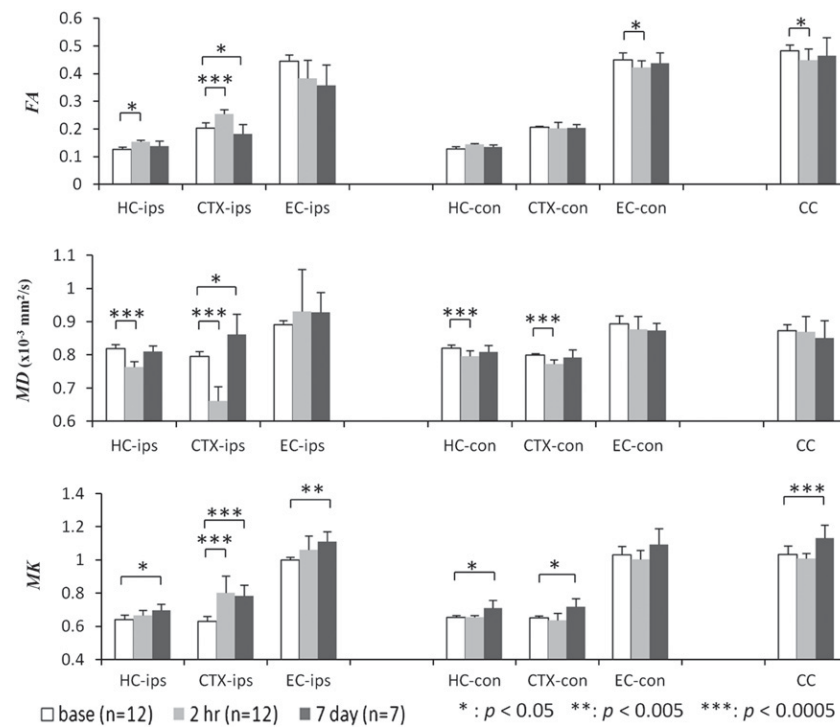


**Fig. 4.** Changes in MD, FA and MK values for ipsilateral and contralateral hippocampus (HC-ips, HC-con), cortex (CTX-ips, CTX-con), external capsule (EC-ips, EC-con), and corpus callosum (CC) from baseline to 7 days post-injury. Statistical significance was based on comparison with baseline values. Error bars indicate standard deviation.

The increase of  $K_a$  in CC on the other hand was significant only at the sub-acute stage ( $p = 0.0084$ ).

The temporal changes in  $K_r$  were significant in all the three white matter regions (EC\_ips:  $F_{2,11} = 6.37$ ,  $p = 0.024$ ; CC:  $F_{2,11} = 6.49$ ,  $p = 0.023$ ; EC\_con:  $F_{2,11} = 6.19$ ,  $p = 0.026$ ). Significant reductions in  $K_r$  were observed in both the CC ( $p = 0.009$ ) and EC\_con ( $p = 0.01$ ) at the acute stage which then returned to the baseline by the sub-acute stage (Fig. 5). A similar trend was also observed in EC\_ips ( $p = 0.07$ ).

It should be noted that while MD was found to be a good discriminator of injury in the cortex and the hippocampus at the acute stage, it was unable to distinguish changes in these brain tissues at the sub-acute stage (HC\_ips:  $p = 0.66$ ; HC\_con:  $p = 0.98$ ; Cor\_con:  $p = 0.97$ ). However, MK was able to distinguish changes in the brain microstructure between the baseline and the sub-acute stage following injury, both in the gray and white matter regions. The increase in MK was also observed in the contralateral hippocampus and the cortex although to a lower extent.

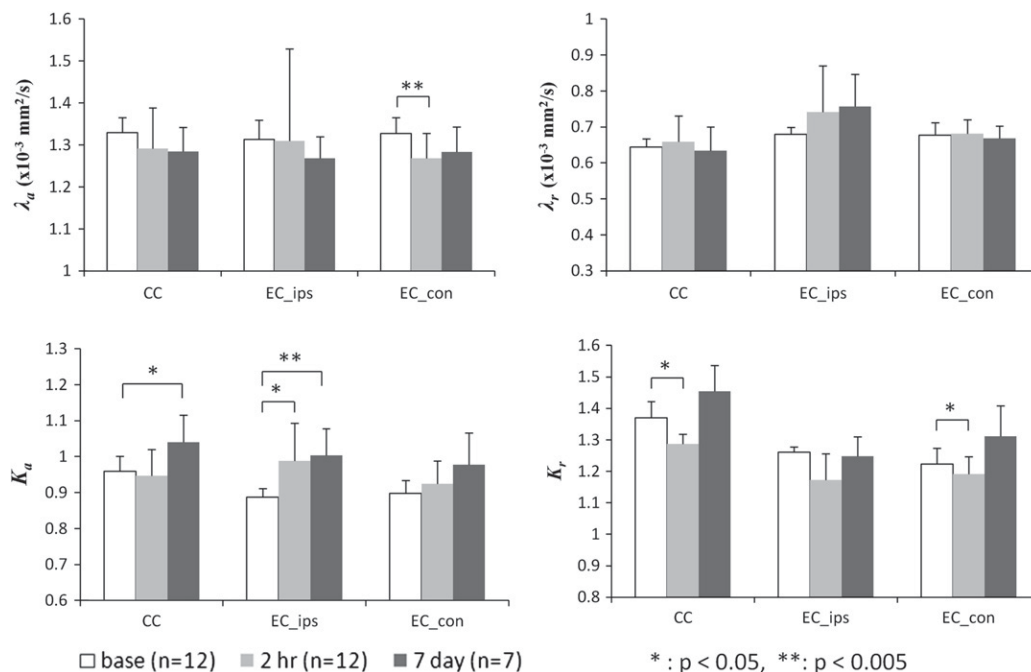


**Fig. 5.** Changes in radial and axial diffusivity ( $\lambda_a$ ,  $\lambda_r$ ), and kurtosis ( $K_a$ ,  $K_r$ ) for white matter regions of corpus callosum (CC) and bi-lateral external capsule (EC\_ips, EC\_con) from baseline to 7 days post-injury. Statistical significance was based on comparison with baseline values. Error bars indicate standard deviation.

Diffusion kurtosis vs. histology

Fig. 6 shows histology using glial fibrillary acidic protein (GFAP) staining from two representative rats (Rat A and B) at the sub-acute stage post injury compared to a sham rat. Significantly increased GFAP immunoreactivity, indicated by increased number of astrocytes, is clearly present for both Rat A and B in the ipsilateral cortex and the hippocampus compared to the sham rat. For rat A, the contralateral side also showed an increased GFAP immunoreactivity, which was associated with increased *MK* values (not accompanied by *MD* values change), indicating that *MK* is sensitive to the changes associated with reactive astrogliosis. For rat B, the contralateral cortex had very low levels of GFAP staining that corresponded with low *MK* values.

To assess the sensitivity of the various DTI/DKI parameters in detecting the abnormality far away from the foci of injury, the rats were divided into two groups based on the density observed in GFAP staining

in the contralateral cortex. Two rats were found to have severe contralateral cortex staining (severe group, like rat A in Fig. 6) and the other five were found to have mild staining in the contralateral cortex (mild group, like rat B in Fig. 6). Fig. 7 shows pair-wise scatter plots for *MD*, *FA* and *MK* (*FA* vs. *MD*, *MK* vs. *FA*, and *MD* vs. *MK*) values from all voxels within the contralateral cortex ROI of all rats in each group along with their respective histograms (20 bins, smoothed by 3 point moving average). The plot of *MK* vs. *MD* for the severe group (Fig. 7a) for the *MK* values compared to the *MD* values between the voxels at baseline and the voxels from the sub-acute stage following injury indicating that *MK* is sensitive to changes associated with reactive astrogliosis. Similarly, an upward shift of *MK* peak is also seen while no shift is observed for *FA*. Fig. 7b shows a similar pair-wise scatter plot for the mildly stained rats. No significant shifts of *MD*, *FA* or *MK* were observed in this group in the contralateral cortex. To compare the changes in voxel values between baseline and the sub-acute stage for the different parameters,

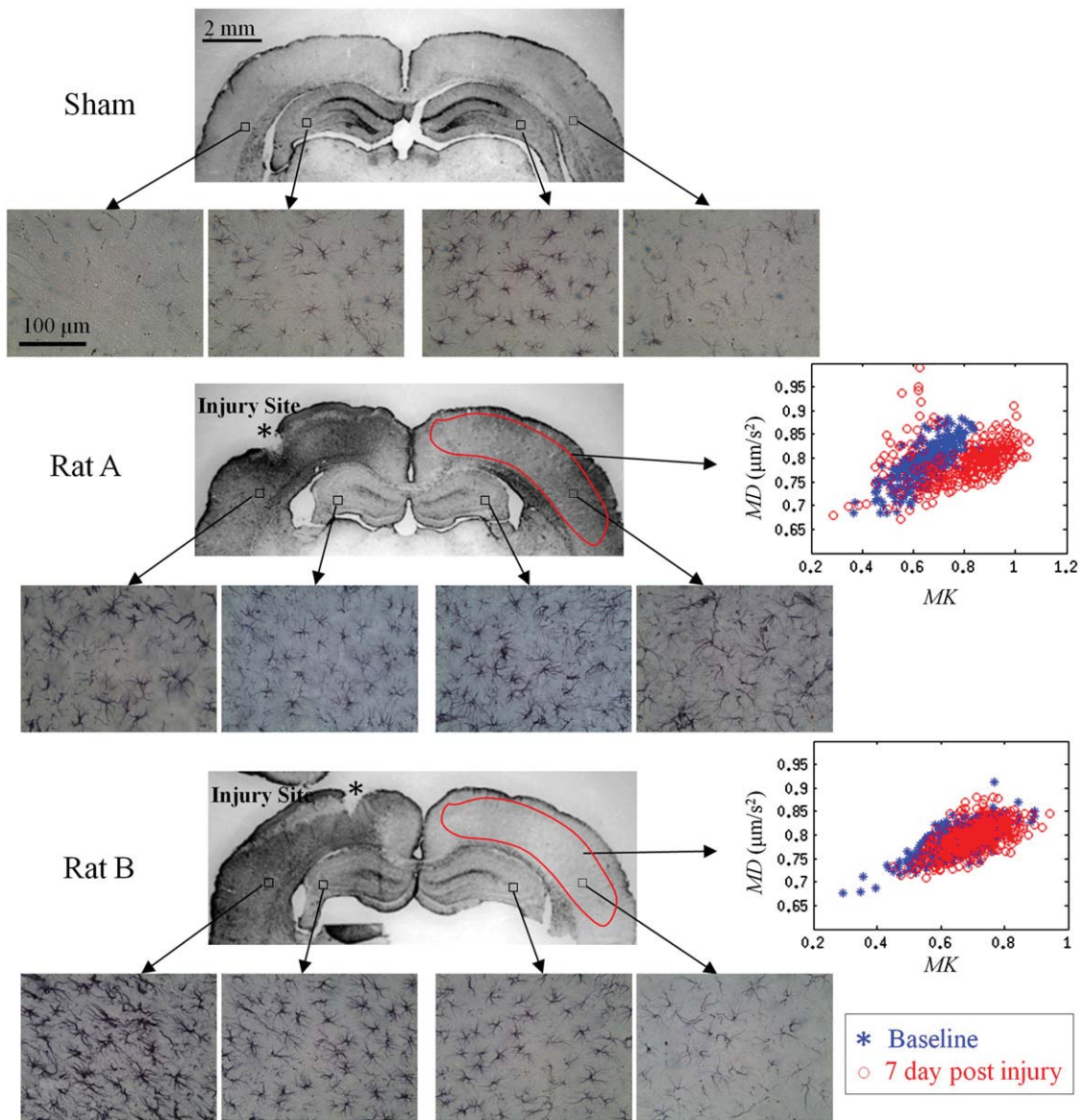
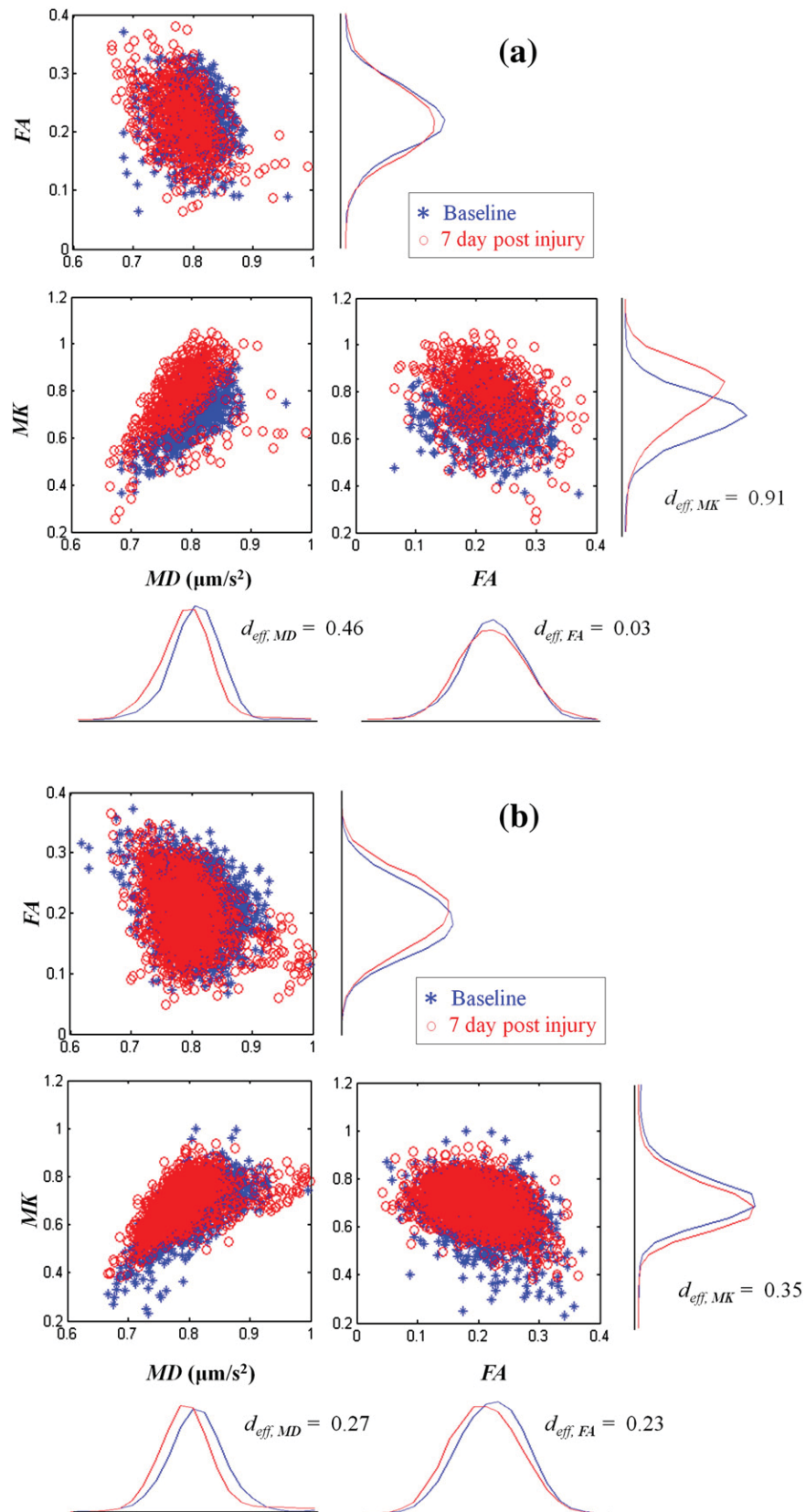


Fig. 6. Comparison of immunohistochemical stains using glial fibrillary acidic protein (GFAP) two representative CCI exposed rats (Rats A and B) at 7 day post-injury and a sham rat. Both Rats A and B expressed significantly increased GFAP immunoreactivity at the site of the injury. However, Rat A also expressed significantly elevated GFAP immunoreactivity compared to Rat B in the contralateral cortex. Also shown are the *MK* vs. *MD* scattered plots from the contralateral cortex of both rats. The GFAP stains (40× magnification) are shown from the ipsilateral cortex, hippocampus and contralateral hippocampus, cortex of each rat. Increased *MK* was associated with increased GFAP staining as in the case of Rat A while it remained the same among rats that did not show elevated GFAP staining as in the case of Rat B. It should be noted that no changes are seen in *MD* for Rat A between the baseline and 7 days post-injury despite an increase in *MK*.



**Fig. 7.** Pair-wise scattered plots of diffusion-related ( $MD$ ,  $FA$ ) and kurtosis-related ( $MK$ ) parameters for voxels from an ROI on the contralateral cortex (see Fig. 2) from groups of (a) severely and (b) mildly stained rats showing changes in these parameters at 7 days post injury (red dots) in comparison to the baseline (blue dots). The corresponding histograms for each of the parameters with the effect size  $d_{\text{eff}}$  are also shown.

standardized mean effect size was computed using Cohen's  $d$  [Cohen, 1988], which is defined as the difference between two means divided by the standard deviation of the data. In this test, an effect size of around 0.8 is considered large, an effect size of 0.5 as moderate and an effect size of 0.2 is considered small [Cohen, 1988]. The effect size between the baseline voxels and the seven day voxels for the severe group was large for  $MK$  ( $d_{\text{eff}, MK} = 0.91$ ), moderate for  $MD$  ( $d_{\text{eff}, MD} = 0.46$ ) and none for  $FA$  ( $d_{\text{eff}, FA} = 0.03$ ). In the mild group, the two clusters of baseline and the sub-acute stage voxel values were not separable by the pair-wise plots, although the histogram indicating a slight shift of  $MD$  and  $FA$  toward lower values, while  $MK$  tended to be higher. However, the overall effect of all three parameters were small ( $d_{\text{eff}, MD \& FA} \approx 0.2$ ), with  $MK$  showing the largest effect ( $d_{\text{eff}, MK} = 0.35$ ). Overall these results suggest that changes in  $MK$  are strongly associated with increased GFAP immunoreactivity.

## Discussion

Diffusion-weighted MRI, and especially DTI, has long been shown to be a powerful tool in detecting tissue microstructure changes in vivo. However, the model most widely used inherently expects diffusion distances to have a Gaussian distribution, which can mask information regarding the underlying tissue heterogeneity. More recently, diffusion kurtosis has been described as an imaging marker that can provide information on tissue heterogeneity or tissue complexity [Jensen and Helpert, 2010] and hence can reveal information beyond measures such as  $MD$  or  $FA$ . Our results indicate that diffusion kurtosis provides additional information not available through standard DTI parameters, and is sensitive to local tissue heterogeneity both in the gray and white matter following traumatic brain injury. More specifically, our study indicates a strong association with diffusion kurtosis and astrocytic immunoreactivity as revealed by the GFAP stains.

In a study of brain maturation, Falangola et al. (2008) have shown that  $MK$  is sensitive to changes in gray matter, where  $MK$  increases with brain maturation while the DTI parameters,  $MD$  and  $FA$  remained relatively unchanged. They postulated that the increase in  $MK$  during maturation in the gray and white matter was likely due to consistent and continuing myelination and an overall increase of the microstructural complexity and increased cell-packing density especially in the gray matter. Post-mortem studies also confirm the increase in the number and volume of glial cells with age in response to neuronal pruning as part of the developmental process of the nervous system [Finch, 2003; Terry et al., 1987]. The combined effect of increased glial cell activity and neuronal pruning may essentially offset any changes in DTI parameters including  $MD$  and  $FA$ . However, this complex scenario of microstructural changes appears to be sensitive to  $MK$ .

Previous studies of brain injury have observed reactive astrogliosis activity to peak at 4–7 days post injury [Chen et al., 2003; Mac Donald et al., 2007]. This observation agrees with our histopathological findings where we observe significant increase in reactive astrocytosis and microglial response at 7 days. Furthermore, this increased reactive astrogliosis corresponds directly to the increased  $MK$  seen in vivo at sub-acute stage when DTI parameters such as  $FA$  and  $MD$  have returned to baseline, indicating that  $MK$  is sensitive to changes in tissue microstructure in response to the injury. Taken together, the results from DKI and histology confirm that  $MK$  is sensitive to the increased complexity of the tissue microstructure in response to the TBI.

Although the primary injury from CCI was focal, the pattern of injury as observed through DKI, especially at the sub-acute stage, was diffuse and even extended to the contralateral hemisphere. This finding is consistent with a previous study that found progressive neurodegeneration following CCI, starting at the site of the injury and gradually progressing to a widespread callosal and thalamic neurodegeneration in both hemispheres by 7 days [Hall et al., 2005]. The authors attributed this widespread change to degeneration of fibers in

the corpus callosum and commissural pathway, causing progressive neuronal death and cellular destruction on the contralateral hemisphere. Reactive astrocytes are also known to have important neuroprotective roles after trauma in preserving neural tissue and restricting inflammation [Chen and Swanson, 2003; Laird et al., 2008; Myer et al., 2006]. So such a process would also likely trigger mild reactive astrogliosis that might contribute to an increase in  $MK$  in the contralateral hemisphere. It is well known that reactive astrogliosis occurs in response to CNS injury and other disease process, the extent of which may vary based on the severity of the insult [Laird et al., 2008; Sofroniew, 2009]. These changes are modulated by inter- and intra-cellular signaling mechanisms and have the potential to modify the degree of changes in a manner that can be either detrimental or beneficial for the surrounding cells. The increased GFAP staining in the contralateral cortex for Rat A in Fig. 6 at the sub-acute stage is indicative of mild to moderate reactive astrogliosis. Although some hypertrophy is observed without intermingling or overlapping of astrocyte domains, it is likely that such proliferation will eventually resolve and the astrocytes will return to their normal appearance [Sofroniew and Vinters, 2010]. Indeed this was the observation made by Chen et al. (2003) in a non-imaging study where a significant proliferation of reactive astrocytes was observed up to 7 days with eventual resolution to normal levels by 28 days post CCI.

The DTI changes in the white matter were more severe in regions adjacent to the direct impact compared to the remote regions in the contralateral hemisphere. A significant reduction in  $FA$  in the corpus callosum and the contralateral external capsule at the acute stage that returned to baseline by 7 days was observed. Further, a trend towards a decrease in  $FA$ , driven by a reduction in  $\lambda_a$  was observed in the ipsilateral external capsule. This behavior appears to be typical of CCI related axonal injury and is consistent with DTI studies in mice using the same injury model [Mac Donald et al., 2007], as well as other diffuse axonal injury studies in human TBIs [Kraus et al., 2007; Mayer et al., 2010]. It should be noted that the experimental injury used in our study was of only 1.5 mm impact depth compared to the more severe impact depth of 2.5 mm used by Mac Donald et al. (2007). This might also explain the relatively milder changes in both  $\lambda_a$  and  $\lambda_r$  in our study.

In the regions of the white matter, we also observed increased  $K_a$  and decreased  $K_r$  associated with decreased and increased diffusivity respectively in their respective directions. This may be due to broken and beading axons, which would cause more water diffusion restriction in the axial direction, leading to lower  $\lambda_a$  and higher  $K_a$ . These processes together with demyelination may result in more free water diffusion in the radial direction and hence higher  $\lambda_r$  and lower  $K_r$ . Moreover, the significant decrease of  $K_r$  within CC and EC\_con at the acute stage is accompanied by no changes in  $\lambda_r$  which further suggests that kurtosis is more sensitive to changes in intra- and extra-axonal water exchange (for example, in the case of axonal break-down and demyelination), as also suggested by Jensen [Jensen and Helpert, 2010]. The increase in  $K_a$  was also significant in the ipsilateral EC without a corresponding change in  $\lambda_a$ . This is probably due to the combined effect of axonal break-down and swelling in the tissue, which could effectively counterbalance, leading to no changes in  $MD$  (Fig. 4), while increasing tissue heterogeneity would still lead to the observed increase in  $MK$  [Jensen et al., 2010]. The increase in  $K_a$  and normalization of  $K_r$  at sub-acute stage can be attributed to reactive fibrous astrogliosis activity in the white matter.

DTI has been used extensively in characterizing white matter disease because diffusion properties along and perpendicular to the axon provide important information about axonal integrity. However, given the isotropic nature of gray matter, studies of microstructural imaging changes in the gray matter have been very limited. The fact that changes in the gray matter can be realized using  $MK$  provides an extra dimension to the repertoire of imaging techniques for the investigators. The directly impacted cortex shows an increased  $MD$

and reduced *FA* at the acute stage due to tissue edema, visible on  $T_2$ -weighted images. In the gray matter regions of the hippocampus and the cortex, we observed a reduced *MD* and increased *FA* at the acute stage. Similar DTI signal behavior has been reported in white matter regions, thalamus and at the whole brain level for TBI patients at the acute stage (Bazarian et al., 2007; Chu et al., 2010; Shanmuganathan et al., 2004; Wilde et al., 2008;) and has been attributed to cell swelling and cytotoxic edema. By the sub-acute stage a return to the baseline for *MD* and *FA* was observed in all these regions. Similar patterns of changes in *MD/FA* at an early and late stage were reported in a longitudinal study of mild TBI patients at 12 days post injury and 3–5 months post-injury respectively (Mayer et al., 2010). Increased *MD* and/or reduced *FA* at the chronic stage has also been observed in both white matter and gray matter in human studies (Bazarian et al., 2007; Kraus et al., 2007; Niogi et al., 2008; Chen and Swanson, 2003, 2008) and also in several animal studies (Immonen et al., 2009; Mac Donald et al., 2007).

Reliance purely on DTI parameters may underestimate the underlying cellular processes that influence changes in the tissue microstructure. In our study, the acute *MK* increase was only significant in the ipsilateral cortex and was directly associated with highly restricted diffusion as observed by *MD* in the directly impacted area. However, a wide spread increase in *MK* was observed by the sub-acute stage in other regions, at a time when both *MD* and *FA* appear to return to baseline levels. The increase in *MK* suggests increased tissue heterogeneity which was confirmed as reactive astrogliosis from GFAP staining. The normalization of *MD* and *FA* may reflect the ongoing activity of both detrimental and beneficial astrogliosis processes, the complexity of which is only reflected by changes in *MK*. Once again, this reflects the sensitivity of *MK* that is not captured by either *MD* or *FA* which underestimate the processes underlying tissue microstructure changes, when clearly reactive protoplasmic astrocytes have not completely resolved.

One limitation to the present study is that only GFAP staining was performed to obtain immunohistochemistry information on the animals. Although our study here clearly indicates an association of increased *MK* to increased reactive astrocyte activity from GFAP staining, one should not discount the possibility of other physiological processes that may also be in play that may have an effect on diffusion kurtosis. For example as indicated earlier, cellular destruction, edema, axonal breakage or demyelination, etc. have been shown to be sensitive to diffusion-weighted imaging, and may also contribute to changes in diffusion kurtosis. While future studies should focus on teasing the contribution of these physiological processes, it is clear that diffusion kurtosis may have value in the case of mild injury where no focal contusion or lesion is observed on conventional MRI or can be identified by standard DTI parameters. Because of its sensitivity to changes in reactive astrogliosis, diffusion kurtosis may be a suitable imaging marker to monitor inflammatory changes in the brain following TBI.

The association of increased *MK* to increased astrocyte immunoreactivity in this study should also be viewed in the context of its limitations. The sample size used in this study is small especially at the sub-acute stage compared to the acute stage (only 7 out of 12 were imaged at 7 day post injury). Although we observed a strong association of changes in *MK* with GFAP immunoreactivity, it would be of great interest to see how *MK* correlates with histological findings, especially with the density of astrocytes within the injured tissue and the relationship with behavior and size of the contusion. It should be noted that reactive astrogliosis is believed to be a reliable and sensitive marker of diseased tissue (Sofroniew and Vinters, 2010) and can play an important role in determining long-term clinical outcome (Chen et al., 2003; Sofroniew, 2009). Another key limitation to our study is that we only followed the animals for 7 days. It would be of interest to see if the *MK* tracks the normalization of the astrocytic activity over a longer period.

We only used three b-values primarily because of concern for the effects of prolonged anesthesia for the animals, potential for the

animal to move during these prolonged experiments, and time constraints posed for magnet use. The reliability in the estimation of DKI parameters increases with the use of multiple b-values as it helps in minimizing fitting errors (Cheung et al., 2009; Falangola et al., 2008; Hui et al., 2008). However, more b-values will have little influence on the standard DTI parameters (Veraart et al., 2011). While the use of only three different b-values up to a maximum b-value of 2000 s/mm<sup>2</sup> may have led to some error in the estimation of the DKI parameters, such an acquisition has been suggested to be more practical in the clinical scenario (Jensen and Helpert, 2010).

## Conclusions

In summary, diffusion kurtosis parameters can provide additional microstructural information and complement the parameters from diffusion tensor imaging. Our study clearly indicates that changes in diffusion kurtosis parameters correspond to active processes that involve reactive astrocytes not realized by other MR imaging techniques. Given that reactive astrogliosis is considered to be a reliable and sensitive biomarker for insults from traumatic brain injury and the fact that it can play an important role in determining the clinical outcome, we believe that DKI parameters are effective imaging markers to detect this activity in vivo.

## Acknowledgments

The authors thank Dr. Lily Wang, University of Georgia for help with statistical analysis, Dr. Jens Jensen, New York University and Dr. Angelos Barmpoutis, University of Florida for their insights into analysis of diffusion kurtosis data. The authors also thank Dr. Yihong Yang, Chief of MRI Section, National Institute of Drug Abuse, for providing useful comments on the manuscript. This work was partly supported by grants from the NIH (1S10RR019935), US Army (W81XWH-07-2-0118 & W81XWH-09-2-0187), and the Office of Naval Research (N000141010886).

## References

- Alexander, A.L., Lee, J.E., Lazar, M., Field, A.S., 2007. Diffusion tensor imaging of the brain. *Neurotherapeutics* 4 (3), 316–329.
- Armitage, P.A., Bastin, M.E., Marshall, L., Wardlaw, J.M., Cannon, J., 1998. Diffusion anisotropy measurements in ischaemic stroke of the human brain. *MAGMA* 6 (1), 28–36.
- Assaf, Y., Cohen, Y., 1998. Non-mono-exponential attenuation of water and N-acetyl aspartate signals due to diffusion in brain tissue. *J. Magn. Reson.* 131 (1), 69–85.
- Assaf, Y., Cohen, Y., 2000. Assignment of the water slow-diffusing component in the central nervous system using q-space diffusion MRS: implications for fiber tract imaging. *Magn. Reson. Med.* 43, 191–199.
- Benjamini, Y., Hochberg, Y., 1995. Controlling the false discovery rate: a practical and powerful approach to multiple testing. *J. R. Statist. Soc. B.* 57 (1), 289–300.
- Bazarian, J.J., Zhong, J., Blyth, B., Zhu, T., Kavcic, V., Peterson, D., 2007. Diffusion tensor imaging detects clinically important axonal damage after mild traumatic brain injury: a pilot study. *J. Neurotrauma* 24 (1), 1447–1459.
- Bulakbasi, N., Kocaoglu, M., Ors, F., Tayfun, C., Uçöz, T., 2003. Combination of single-voxel proton MR spectroscopy and apparent diffusion coefficient calculation in the evaluation of common brain tumors. *AJNR Am. J. Neuroradiol.* 24 (2), 225–233.
- Cercignani, M., Bozzali, M., Iannucci, G., Comi, G., Filippi, M., 2001. Magnetisation transfer ratio and mean diffusivity of normal appearing white and grey matter from patients with multiple sclerosis. *J. Neurol. Neurosurg. Psychiatr.* 70 (3), 311–317 (PMID:11181851).
- Chen, S., Pickard, J.D., Harris, N.G., 2003. Time course of cellular pathology after controlled cortical impact injury. *Exp. Neurol.* 182 (1), 87–102.
- Chen, Y., Swanson, R.A., 2003. Astrocytes and brain injury. *J. Cereb. Blood Flow Metab.* 23, 137–149.
- Cheung, M.M., Hui, E.S., Chan, K.C., Helpert, J.A., Qi, L., Wu, E.X., 2009. Does diffusion kurtosis imaging lead to better neural tissue characterization? A rodent brain maturation study. *NeuroImage* 45, 386–392.
- Chu, Z., Wilde, E.A., Hunter, J.V., McCauley, S.R., Bigler, E.D., Troyanskaya, M., et al., 2010. Voxel-based analysis of diffusion tensor imaging in mild traumatic brain injury in adolescents. *AJNR Am. J. Neuroradiol.* 31, 340–346.
- Cohen, J., 1988. *Statistical Power Analysis for the Behavioral Sciences* 2nd ed. Routledge Academic 9780805802832.
- Cohen, Y., Assaf, Y., 2002. High b-value q-space analyzed diffusion-weighted MRS and MRI in neuronal tissues – a technical review. *NMR Biomed.* 15 (7–8), 516–542.

- Cox, R.W., 1996. AFNI: software for analysis and visualization of functional magnetic resonance neuroimages. *Comput. Biomed. Res.* 29 (3), 162–173 Jun.
- Dixon, C.E., Clifton, G.L., Lighthall, J.W., Yaghmai, A.A., Hayes, R.L., 1991. A controlled cortical impact model of traumatic brain injury in the rat. *J. Neurosci. Methods* 39, 253–262.
- Falangola, M.F., Jensen, J.H., Babb, J.S., Hu, C., Castellanos, F.X., Di Martino, A., et al., 2008. Age-related non-Gaussian diffusion patterns in the prefrontal brain. *J. Magn. Reson. Imaging* 28, 1345–1350.
- Farrell, J.A., Zhang, J., Jones, M.V., Deboy, C.A., Hoffman, P.N., Landman, B.A., et al., 2010. q-space and conventional diffusion imaging of axon and myelin damage in the rat spinal cord after axotomy. *Magn. Reson. Med.* 63 (5), 1323–1335.
- Finch, C.E., 2003. Neurons, glia, and plasticity in normal brain aging. *Neurobiol. Aging* 24 (Suppl 1), S123–S127.
- Guo, A.C., Cummings, T.J., Dash, R.C., Provenzale, J.M., 2002. Lymphomas and high-grade astrocytomas: comparison of water diffusibility and histologic characteristics. *Radiology* 224, 177–183.
- Hall, E.D., Sullivan, P.G., Gibson, T.R., Pavel, K.M., Thompson, B.M., Scheff, S.W., 2005. Spatial and temporal characteristics of neurodegeneration after controlled cortical impact in mice: more than a focal brain injury. *J. Neurotrauma* 22 (2), 252–265 Feb.
- Hui, E.S., Cheung, M.M., Qi, L., Wu, E.X., 2008. Towards better MR characterization of neural tissues using directional diffusion kurtosis analysis. *NeuroImage* 42, 122–134.
- Immonen, R.J., Kharatishvili, I., Niskanen, J.P., Gröhn, H., Pitkänen, A., Gröhn, O.H., 2009. Distinct MRI pattern in lesional and perilesional area after traumatic brain injury in rat—11 months follow-up. *Exp. Neurol.* 215, 29–40.
- Jansen, J.F., Stambuk, H.E., Koutcher, J.A., Shukla-Dave, A., 2010. Non-Gaussian analysis of diffusion-weighted MR imaging in head and neck squamous cell carcinoma: a feasibility study. *AJNR Am. J. Neuroradiol.* 31, 741–748.
- Jensen, J.H., Helpert, J.A., Ramani, A., Lu, H., Kaczynski, K., 2005. Diffusional kurtosis imaging: the quantification of non-Gaussian water diffusion by means of magnetic resonance imaging. *Magn. Reson. Med.* 53, 1432–1440.
- Jensen, J.H., Helpert, J.A., 2010. MRI quantification of non-Gaussian water diffusion by kurtosis analysis. *NMR Biomed.* 23 (7), 698–710.
- Jiang, Q., Qu, C., Chopp, M., Ding, G.L., Davarani, S.P., Helpert, J.A., Jensen, J.H., Zhang, Z.G., Li, L., Lu, M., Kaplan, D., Hu, J., Shen, Y., Kou, Z., Li, Q., Wang, S., Mahmood, A., 2011. MRI evaluation of axonal reorganization after bone marrow stromal cell treatment of traumatic brain injury. *NMR Biomed.* doi:10.1002/nbm.1667 Mar 23. [Epub ahead of print].
- Kiselev, V.G., Il'yasov, K.A., 2007. Is the “biexponential diffusion” biexponential? *Magn. Reson. Med.* 57 (3), 464–469.
- Kraus, M.F., Susmaras, T., Caughlin, B.P., Walker, C.J., Sweeney, J.A., Little, D.M., 2007. White matter integrity and cognition in chronic traumatic brain injury: a diffusion tensor imaging study. *Brain* 130 (Pt 10), 2508–2519.
- Laird, M.D., Vender, J.R., Dhandapani, K.M., 2008. Opposing roles for reactive astrocytes following traumatic brain injury. *Neurosignals* 16 (2–3), 154–164.
- Lu, H., Jensen, J.H., Ramani, A., Helpert, J.A., 2006. Three-dimensional characterization of non-Gaussian water diffusion in humans using diffusion kurtosis imaging. *NMR Biomed.* 19, 236–247.
- Mac Donald, C.L., Dikranian, K., Bayly, P., Holtzman, D., Brody, D., 2007. Diffusion tensor imaging reliably detects experimental traumatic axonal injury and indicates approximate time of injury. *J. Neurosci.* 27, 11869–11876.
- Mayer, A.R., Ling, J., Mannell, M.V., Gasparovic, C., Phillips, J.P., Doezema, D., et al., 2010. A prospective diffusion tensor imaging study in mild traumatic brain injury. *Neurology* 74, 643–650.
- Maier, S.E., Bogner, P., Bajzic, G., Mamata, H., Mamata, Y., Repa, I., et al., 2001. Normal brain and brain tumor: multicomponent apparent diffusion coefficient line scan imaging. *Radiology* 219, 842–849.
- Maier, S.E., Vajapeyam, S., Mamata, H., Westin, C.F., Jolesz, F.A., Mulkern, R.V., 2004. Biexponential diffusion tensor analysis of human brain diffusion data. *Magn. Reson. Med.* 51 (2), 321–330.
- Maier, S.E., Mulkern, R.V., 2008. Biexponential analysis of diffusion-related signal decay in normal human cortical and deep gray matter. *Magn. Reson. Imaging* 26, 897–904.
- Milne, M.L., Conradi, M.S., 2009. Multi-exponential signal decay from diffusion in a single compartment. *J. Magn. Reson.* 197 (1), 87–90 (PMID:19121965).
- Mulkern, R.V., Gudbjartsson, H., Westin, C.F., Zengingonul, H.P., Gartner, W., Guttmann, C.R., et al., 1999. Multicomponent apparent diffusion coefficients in human brain. *NMR Biomed.* 12, 51–62.
- Myer, D.J., Gurkoff, G.G., Lee, S.M., Hovda, D.A., Sofroniew, M.V., 2006. Essential protective roles of reactive astrocytes in traumatic brain injury. *Brain* 129, 2761–2772.
- Newcombe, V.F., Williams, G.B., Nortje, J., Bradley, P.G., Harding, S.G., Smielewski, P., et al., 2007. Analysis of acute traumatic axonal injury using diffusion tensor imaging. *Br. J. Neurosurg.* 21 (4), 340–348.
- Niendorf, T., Dijkhuizen, R.M., Norris, D.G., van Lookeren Campagne, M., Nicolay, K., 1996. Biexponential diffusion attenuation in various states of brain tissue: implications for diffusion-weighted imaging. *Magn. Reson. Med.* 36, 847–857.
- Niogi, S.N., Mukherjee, P., Ghajar, J., Johnson, C., Kolster, R.A., Sarkar, R., Lee, H., Meeker, M., Zimmerman, R.D., Manly, G.T., McCandless, B.D., 2008. Extent of microstructural white matter injury in postconcussive syndrome correlates with impaired cognitive reaction time: a 3T diffusion tensor imaging study of mild traumatic brain injury. *AJNR Am. J. Neuroradiol.* 29 (5), 967–973 (PMID 18272556).
- Paxinos, G., Watson, C., 1986. *The Rat Brain in Stereotaxic Coordinates*. Academic Press Inc.
- Pierpaoli, C., Jezzard, P., Basser, P.J., Barnett, A., Di Chiro, G., 1996. Diffusion tensor MR imaging of the human brain. *Radiology* 201, 637–648.
- Raab, P., Hattingen, E., Franz, K., Zanella, F.E., Lanfermann, H., 2010. Cerebral gliomas: diffusional kurtosis imaging analysis of microstructural differences. *Radiology* 254, 876–881.
- Sidaros, A., Engberg, A.W., Sidaros, K., Liptrot, M.G., Herning, M., Petersen, P., et al., 2008. Diffusion tensor imaging during recovery from severe traumatic brain injury and relation to clinical outcome: a longitudinal study. *Brain* 131 (Pt 2), 559–572.
- Shanmuganathan, K., Gullapalli, R.P., Mirvis, S.E., Roys, S., Murthy, P., 2004. Whole brain apparent diffusion coefficient in traumatic brain injury: correlation with Glasgow Coma Scale score. *AJNR Am. J. Neuroradiol.* 25, 539–544.
- Shaw, G., 2010. New imaging captures the brain's complexity. *Neurology Now* 9–10.
- Sofroniew, M.V., 2009. Molecular dissection of reactive astrogliosis and glial scar formation. *Trends Neurosci.* 32, 638–647.
- Sofroniew, M.V., Vinters, H.V., 2010. Astrocytes: biology and pathology. *Acta Neuropathol.* 119, 7–35.
- Song, S.K., Sun, S.W., Ju, W.K., Lin, S.J., Cross, A.H., Neufeld, A.H., 2003. Diffusion tensor imaging detects and differentiates axon and myelin degeneration in mouse optic nerve after retinal ischemia. *NeuroImage* 20, 1714–1722.
- Terry, R.D., DeTeresa, R., Hansen, L.A., 1987. Neocortical cell counts in normal human adult aging. *Ann. Neurol.* 21 (6), 530–539.
- Trampel, R., Jensen, J.H., Lee, R.F., Kamenetskiy, I., McGuinness, G., Johnson, G., 2006. Diffusional kurtosis imaging in the lung using hyperpolarized <sup>3</sup>He. *Magn. Reson. Med.* 56, 733–737.
- Veraart, J., Poot, D.H., Van Hecke, W., Blockx, I., Van der Linden, A., Verhoye, M., Sijbers, J., 2011. More accurate estimation of diffusion tensor parameters using diffusion kurtosis imaging. *Magn. Reson. Med.* 65 (1), 138–145.
- Wieshmann, U.C., Clark, C.A., Symms, M.R., Franconi, F., Barker, G.J., Shorvon, S.D., 1999. Anisotropy of water diffusion in corona radiata and cerebral peduncle in patients with hemiparesis. *NeuroImage* 10 (2), 225–530 (PMID:10417255).
- Wilde, E.A., McCauley, S.R., Hunter, J.V., Bigler, E.D., Chu, Z., Wang, Z.J., et al., 2008. Diffusion tensor imaging of acute mild traumatic brain injury in adolescents. *Neurology* 70, 948–955.
- Wu, E.X., Cheung, M.M., 2010. MR diffusion kurtosis imaging for neural tissue characterization. *NMR Biomed.* 23 (7), 836–848.
- Zelaya, F., Flood, N., Chalk, J.B., Wang, D., Doddrell, D.M., Strugnelli, W., Benson, M., Ostergaard, L., Semple, J., Eagle, S., 1999. An evaluation of the time dependence of the anisotropy of the water diffusion tensor in acute human ischemia. *Magn. Reson. Imaging* 17 (3), 331–348 (PMID:10195576).
- Zhuo, J., Simon, J.Z., Gullapalli, R., 2011. Diffusion kurtosis imaging (DKI) reconstruction — linear or non-linear. *Proceedings: International Society for Magnetic Resonance in Medicine, 19th Scientific Meeting, Montreal, Quebec, Canada, p. 6633.*